



HAL
open science

The magnetic field and wind confinement of theta1 Orionis C

Jean-François Donati, J. Babel, Tim J. Harries, I. D. Howarth, Pascal Petit,
Meir Semel

► **To cite this version:**

Jean-François Donati, J. Babel, Tim J. Harries, I. D. Howarth, Pascal Petit, et al.. The magnetic field and wind confinement of theta1 Orionis C. *Monthly Notices of the Royal Astronomical Society*, 2002, 333, pp.55-70. 10.1046/j.1365-8711.2002.05379.x . hal-03801401

HAL Id: hal-03801401

<https://hal.science/hal-03801401>

Submitted on 11 Oct 2022

HAL is a multi-disciplinary open access archive for the deposit and dissemination of scientific research documents, whether they are published or not. The documents may come from teaching and research institutions in France or abroad, or from public or private research centers.

L'archive ouverte pluridisciplinaire **HAL**, est destinée au dépôt et à la diffusion de documents scientifiques de niveau recherche, publiés ou non, émanant des établissements d'enseignement et de recherche français ou étrangers, des laboratoires publics ou privés.

The magnetic field and wind confinement of θ^1 Orionis C

J.-F. Donati,^{1★} J. Babel,^{2★} T. J. Harries,^{3★} I. D. Howarth,^{4★} P. Petit^{1★} and M. Semel^{5★}

¹Laboratoire d'Astrophysique, Observatoire Midi-Pyrénées, 14 Av. E. Belin, F-31400 Toulouse, France

²36 rue des Battieux 2000 Neuchâtel, Switzerland

³School of Physics, University of Exeter, Stocker Road, Exeter EX4 4QL

⁴Department of Physics and Astronomy, University College of London, London

⁵DASOP, Observatoire de Paris-Meudon, 5 place J. Janssen, F-92195 Meudon Principal Cédex, France

Accepted 2002 January 31. Received 2002 January 28; in original form 2001 December 3

ABSTRACT

We report the detection, through spectropolarimetric observations, of a strong dipolar magnetic field of presumably fossil origin at the surface of the very young O star θ^1 Ori C. The Stokes V signatures we detect are variable with time, the variations being consistent with rotational modulation. A detailed modelling of our observations indicates that this dipole field has an intensity of 1.1 ± 0.1 kG and is inclined at $42^\circ \pm 6^\circ$ with respect to the rotation axis (assumed to be inclined at 45° to the line of sight). We find, in particular, that the positive magnetic pole comes closest to the observer when the variable $H\alpha$ emission component observed on this star reaches maximum strength. This discovery represents the first definite detection of a magnetic field in an O star, as well as the first detection of a fossil field in a very young star.

We also investigate in this paper the magnetic confinement of the radiatively driven wind of θ^1 Ori C in the context of the magnetically confined wind-shock model of Babel & Montmerle. In the case of θ^1 Ori C, this model predicts the formation of a large magnetosphere (extending as far as $2-3R_*$), consisting of a very hot post-shock region (with temperatures in excess of 10 MK and densities of about $10^{10}-10^{11}$ cm⁻³) generated by the strong collision of the wind streams from both stellar magnetic hemispheres, as well as a dense cooling disc forming in the magnetospheric equator. We find that this model includes most of the physics required to obtain a satisfactory level of agreement with the extensive data sets available for θ^1 Ori C in the literature (and, in particular, with the recent X-ray data and the phase-resolved spectroscopic observations of ultraviolet and optical wind lines) provided that the mass-loss rate of θ^1 Ori C is at least 5 times smaller than that predicted by radiatively driven wind models. We finally show how new observations with the *XMM* or *Chandra* spacecraft could help us constrain this model much more tightly and thus obtain a clear picture of how magnetic fields can influence the winds of hot stars.

Key words: stars: individual: θ^1 Ori C – stars: magnetic fields – stars: rotation – stars: winds, outflows.

1 INTRODUCTION

As the hottest member of the Orion Trapezium, θ^1 Orionis C (HD 37022, variable spectral type O4-6V) represents the main source of ionizing photons for the entire surrounding nebula. With an age of only about 200 000 yr, it is also one of the youngest, and thus one of the few truly zero-age main-sequence O stars known in the sky (Howarth & Prinja 1989). Although the spectroscopic variability of

θ^1 Ori C was discovered long ago (Conti 1972), it is only relatively recently that Stahl et al. (1993) realized that the spectral lines of this star are actually all varying in a strictly periodic way, with a period of 15.4 d. Further investigations (Walborn & Nichols 1994; Stahl et al. 1996; Stahl 1998) led to an accurate determination of this period (15.426 d), usually assumed to be the rotation period of the star. By analogy with magnetic chemically peculiar (CP) stars featuring similar phenomenology, Stahl et al. (1996) suggested that this modulation is the result of a magnetic structure permeating the stellar atmosphere.

The detection of hard X-ray emission from θ^1 Ori C at a level stronger than that of an average O star, and featuring periodic

★E-mail: jean-francois.donati@obs-mip.fr (J-FD); petit@obs-mip.fr (PP); babeljr@bluewin.ch (JB); th@astro.ex.ac.uk (TJH); idh@star.ucl.ac.uk (IDH); semel@obspm.fr (MS)

variability with the same 15.426-d time-scale (Caillault, Gagné & Stauffer 1994; Gagné et al. 1997), has further enhanced the interest of the hot-star community in this target, as a challenging test bench for theoretical studies of radiatively driven stellar winds and wind shocks in very hot stars. Until very recently, the general belief was that X-ray emission from hot stars arises from shocks that develop in the outflowing stellar wind owing to instabilities associated with the line-driven wind mechanism (Lucy & White 1980; Owocki, Castor & Rybicki 1988; Feldmeier 1995). It is, however, becoming increasingly clear that early B stars emit far more X-rays than this model can explain (e.g. Cohen, Finley & Cassinelli 2002). The most recent X-ray spectroscopic observations of hot stars obtained with the *Chandra* spacecraft (Schulz et al. 2000, 2001 in the particular case of θ^1 Ori C; Waldron & Cassinelli 2001 for the cooler star ζ Ori) indicate that the hard X-ray emission originates from a small and dense region located very close to the stellar surface, in complete contradiction to the standard model that predicts high-energy radiation to come from the outer wind regions. The profiles of X-ray spectral lines also disagree strongly with those expected from the wind-shock model.

Babel & Montmerle (1997b) were the first to propose that the X-ray radiation of θ^1 Ori C is the result of a shock in a magnetically confined wind, thus strengthening the analogy with chemically peculiar stars for which their model (dubbed the magnetically confined wind-shock or MCWS model) was initially designed (Babel & Montmerle 1997a). In this model, the wind streams from both magnetic hemispheres collide with each other, producing a strong shock, an extended X-ray-emitting post-shock region and a thin cooling disc located in the magnetic equatorial plane. In their original paper, Babel & Montmerle (1997b) demonstrated that this model can reproduce the characteristics of the X-ray radiation reasonably well as detected by instruments aboard the *ROSAT* X-ray satellite, provided that the magnetic field at the surface of θ^1 Ori C was of the order of a few hundred G. Furthermore, their model could possibly explain the rotational modulation of the X-ray luminosity through a partial eclipse of the magnetosphere effect by the cooling disc. More recently, Donati et al. (2001) established that this model is also very successful at explaining the *ROSAT* observations of β Cep (on which a magnetic field was detected by Henrichs et al. 2002) and also provides new hints for interpreting the Be episodes that this star undergoes periodically.

An obvious and crucial observational test of this model consists of detecting the magnetic field of θ^1 Ori C and estimating its large-scale structure. From indirect indicators, Stahl et al. (1996) suggest that the field is a magnetic dipole, the axis of which is tilted with respect to the rotation axis by about 45° , the rotation axis being inclined at 45° to the line of sight; in this context, the magnetic dipole should be alternatively aligned (at phase 0.5 in the reference ephemeris of Stahl 1998) and perpendicular (at phase 0.0) to the line of sight. However, attempts at a direct detection of the Zeeman signatures of θ^1 Ori C (e.g. Donati & Wade 1999) have always failed up to now. The main cause for this failure is that such signatures are very weak in O stars (of the order of 0.1 per cent peak to peak for a non-rotating star with a 1-kG dipole field), essentially owing to the fact that the intrinsic profiles of these objects are rather broad (typically several tens of km s^{-1}). Even the newest multiline techniques such as least-squares deconvolution (Donati et al. 1997) only improve the situation marginally given the very few spectral lines suitable for this purpose in the spectrum of an O-type star. For this very reason and despite the relative brightness of θ^1 Ori C, the most sensitive attempt (Donati & Wade

1999) reports one-sigma error bars in the line-of-sight projected (i.e. longitudinal) component of the magnetic field of no smaller than about 250 G, which translates into an upper limit of the polar dipole field strength of slightly less than 2 kG.

In this new paper, we report new spectropolarimetric observations of θ^1 Ori C with unprecedented sensitivity, obtained at the Anglo-Australian Telescope (AAT). After a brief description of these observations, we demonstrate that Zeeman signatures are clearly detected and derive quantitative information on the strength and large-scale geometry of the magnetic field permeating the photosphere of θ^1 Ori C. We then discuss the implications of these new measurements in the context of the MCWS model, and more generally for our understanding of the impact of magnetic fields on the radiatively driven winds of very hot stars.

2 OBSERVATIONS

Observations were carried out in 1999 December and 2000 December at the 3.9-m Anglo-Australian Telescope, with an instrumental setup similar to that described in Donati et al. (2002). A visitor polarimeter is mounted at the Cassegrain focus and linked to the UCL echelle spectrograph through a double optical fibre and a Bowen–Walraven image slicer. With the $31.6 \text{ line mm}^{-1}$ grating and the MITLL2 charge-coupled device (CCD), a resolution of about 60 000 is achieved in a continuous wavelength domain spanning 430–715 nm. Each polarimetric exposure consists of a sequence of four individual subexposures secured at different azimuths of the quarter-wave plate, and processed with specific reduction software as described in Donati et al. (1997).

A total of 19 polarization exposures were recorded on five different nights. As in Donati & Wade (1999), the new multiline technique of least-squares deconvolution (LSD, Donati et al. 1997) was applied to all spectra. Given the fact that we wish to estimate the magnetic field at the stellar surface, we selected only photospheric lines; moreover, only the narrowest of those were kept to minimize blurring of potential Zeeman signatures by broad intrinsic profiles. A careful analysis of the spectrum actually reveals that most of the polarization information actually comes from three main spectral lines, namely the O III line at 559.225 nm and the twin C IV lines at 580.131 and 581.197 nm with respective Landé factors of 1.00, 1.17 and 1.33. Stokes V LSD signatures were thus produced from the four profiles corresponding to these three lines (the O III line showing up in the overlap region of two successive orders). The average wavelength and Landé factor of the resulting mean profile are, respectively, equal to 570 nm and 1.085. A complete log of the observations is given in Table 1.

Given the very small phase variation of θ^1 Ori C within each night of observation (always smaller than 1.3 per cent of a cycle), averaging all LSD profiles recorded in the same night enables us to further decrease the noise level in the polarization spectra without rotationally blurring Zeeman signatures. We therefore end up with five mean LSD profiles (corresponding to rotational phases of 0.033, 0.621, 0.789, 0.920 and 0.177) with respective noise levels as low as 0.021, 0.016, 0.020, 0.028 and 0.032 per cent per 8 km s^{-1} bin. Definite magnetic detections are obtained at all phases except the second one, with reduced χ^2 values within the 21 spectral points of the line profile equal to 2.6, 1.0, 1.9, 1.7 and 1.5, respectively. Note that the non-detection at phase 0.621 is not a result of lower quality data; the noise level achieved on this night is actually the lowest of the whole data set, indicating that the longitudinal field of θ^1 Ori C is genuinely very weak at that phase

Table 1. Journal of observations. The successive columns, respectively, list, for each polarization exposure, the UT and Julian dates, the exposure time t_{exp} , the rotational phase ϕ (using the ephemeris $\text{JD} = 2448833.0 + 15.426E$ of Stahl 1998), the peak S/N ratio per 2 km s^{-1} pixel in the raw spectrum, and the relative rms noise level N_{LSD} per 8 km s^{-1} velocity bin in the resulting LSD Stokes V spectra (see Section 3).

Date	JD 2,451,000+	t_{exp} (min)	ϕ	S/N (pixel $^{-1}$)	N_{LSD} (per cent)
1999 Dec. 20	532.9584	40	0.026	540	0.045
	532.9900	40	0.028	560	0.044
	533.1195	40	0.037	630	0.039
	533.1508	40	0.039	610	0.041
1999 Dec. 29	542.0922	40	0.619	720	0.032
	542.1229	40	0.621	850	0.029
	542.1536	40	0.623	940	0.025
2000 Dec. 05	884.0527	40	0.786	740	0.032
	884.0837	40	0.788	680	0.036
	884.1147	40	0.790	580	0.042
	884.1830	40	0.795	540	0.046
2000 Dec. 07	886.0180	40	0.914	300	0.100
	886.0492	40	0.916	180	0.146
	886.0808	40	0.918	390	0.064
	886.1119	40	0.920	620	0.041
	886.1814	40	0.924	250	0.123
2000 Dec. 11	886.2126	40	0.926	410	0.064
	890.0714	40	0.177	640	0.039
	890.1037	40	0.179	480	0.058

LSD profiles of θ^1 Ori C, AAT, 1999 Dec. 20 & 29

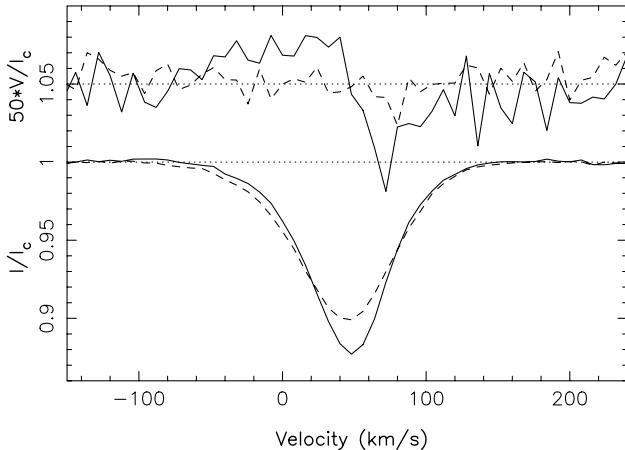


Figure 1. Average Stokes I (bottom curves) and V LSD profiles of θ^1 Ori C at rotational phase 0.033 (full line) and 0.621 (dashed line). Note that Stokes V profiles were expanded by a factor of 50 and shifted upwards by 1.05 for clarity.

of the rotation cycle. The LSD profiles with strongest and weakest magnetic signals (recorded, respectively, on 1999 December 20 and 29, i.e. on rotational phases 0.033 and 0.621) are shown in Fig. 1.

3 STELLAR AND ORBITAL PARAMETERS

Before commencing the detailed analysis of the detected Zeeman signatures, it is important to have as clear an idea as possible of the fundamental parameters of θ^1 Ori C. This allows us not only to constrain the magnetic model, but also to check whether the structure we obtain is compatible with the various observables reported in the literature.

3.1 Fundamental parameters

From the strength of ultraviolet (UV) spectral lines, Howarth & Prinja (1989) conclude that θ^1 Ori C has an effective temperature of about $45000 \pm 1000 \text{ K}$, which corresponds to a bolometric correction of -4.0 ± 0.1 (Howarth & Prinja 1989; Bessel, Castelli & Plez 1998). Given the visual magnitude ($m_V = 5.12$), extinction coefficient ($A_V = 1.6 \pm 0.1$, O'Dell & Yusef-Zadeh 2000) and distance ($450 \pm 50 \text{ pc}$, Genzel & Stutzki 1989; de Zeeuw, Hoogerwerf & de Bruijne 1999) of θ^1 Ori C, we derive that this star is 5.4 ± 0.1 dex more luminous than the Sun, with a radius of $8.2 \pm 1.1 R_\odot$. From a comparison of its location in the Hertzsprung–Russell (HR) diagram with the evolutionary tracks for solar metallicity of Schaller et al. (1992) and Bernasconi & Maeder (1996), we obtain that θ^1 Ori C is a star with a mass of about $44 \pm 5 M_\odot$ and an age of less than 0.6 Myr. This is in good agreement with the earlier determination of Howarth & Prinja (1989), as well as with the estimated age of the Orion Nebula cluster region (Ori OB1d) according to Brown, de Geus & de Zeeuw (1994). Our parameters are, however, incompatible with those assumed by Reiners et al. (2000) in their recent study of the spectroscopic variability of θ^1 Ori C.

In this context, the most recent determination of the rotation period ($15.426 \pm 0.001 \text{ d}$, Stahl 1998) implies an equatorial rotation velocity of $27 \pm 3 \text{ km s}^{-1}$. From the line-of-sight projected rotation velocity estimate of Stahl et al. (1996, $v \sin i = 20 \text{ km s}^{-1}$), we derive that the rotation axis of θ^1 Ori C is inclined at an angle of about $i = 45^\circ$ to the line of sight. However, this parameter is not precisely determined; while the semi-amplitude of radial velocity variations at a given epoch (at least 12 km s^{-1} , Stahl et al. 1996; Stahl 1998) indicates that i must be larger than 25° , the rotational modulation of optical and UV wind lines (showing only one maximum per cycle, around phase 0.0; Stahl et al. 1996) suggests (by comparison with magnetic CP stars) that the observer obtains a very different view of both magnetic poles and therefore that the maximum angle between the rotation axis and the line of sight is significantly lower than 90° (of the order of 65°).

Although θ^1 Ori C has long been suspected to be a spectroscopic binary from low dispersion data (Plaskett & Pearce 1924; Frost, Barrett & Struve 1926), subsequent investigations with higher-dispersion spectrographs (e.g. Conti 1972) are not adequate to confirm this claim. It is only very recently that Stahl (1998) reported definite evidence for radial velocity variations of θ^1 Ori C, with a steady increase in radial velocity (averaged over the rotation cycle) from about 10 km s^{-1} in 1992 up to 35 km s^{-1} in 1997. Our latest observations confirm this trend, with mean radial velocities of about 45 km s^{-1} in late 1999 and 2000. This large-amplitude radial velocity variation therefore strongly argues in favour of θ^1 Ori C indeed being a spectroscopic binary, with an orbital period of at least 8 yr in the case of a highly eccentric orbit and larger than 16 yr if the orbit is circular. The very close visual companion (with a mass of less than $6 M_\odot$) detected recently by Weigelt et al. (1999) through speckle interferometry at 16 au south-west of θ^1 Ori C is certainly a very good candidate for the spectroscopic companion of θ^1 Ori C. This minimum distance of 16 au between components implies a minimum orbital period of about 9 yr, compatible with the observations. However, the corresponding radial velocity variations, assuming a circular orbit, are about twice as small as those observed; one therefore needs to invoke a very eccentric orbit (with an eccentricity of at least 0.85) to obtain a rough match to the observed amplitude of radial velocity variations. If this is the case, both the radial velocities and the separation between system

components should soon undergo very rapid variations. Future spectroscopic and interferometric observations will be necessary to confirm this prediction.

3.2 Wind characteristics

The mass-loss rate estimated for θ^1 Ori C by Howarth & Prinja (1989) from the observation of UV wind lines (and assuming a spherically symmetric wind) is equal to $4 \times 10^{-7} M_{\odot} \text{ yr}^{-1}$ with a rms uncertainty of about a factor of 2. This is in reasonable agreement with their own empirical relation from a fit to both radio and UV observations of O stars (yielding $5 \times 10^{-7} M_{\odot} \text{ yr}^{-1}$ for an O-type star as bright as θ^1 Ori C) as well as with the laminar radiatively driven wind models of Pauldrach, Puls & Kudritzki (1986), predicting a mass-loss rate \dot{M} of $7 \times 10^{-7} M_{\odot} \text{ yr}^{-1}$ for stars similar to θ^1 Ori C. From the maximum velocity measured from the blue wing of C IV lines, Stahl et al. (1996) derive a wind terminal velocity v_{∞} larger than 2500 km s^{-1} , i.e. more than twice the escape velocity (equal to 1300 km s^{-1} for θ^1 Ori C). This is again compatible with the theoretical models of Pauldrach et al. (1986), predicting wind terminal to escape velocity ratios of the order of 3 for stars as hot as θ^1 Ori C.

As already mentioned in the introduction, another parameter of interest in the context of wind models is the X-ray luminosity and variability of θ^1 Ori C. The latest X-ray observations secured by the High-Energy Transmission Grating Spectrometer (HETGS) on board the *Chandra* spacecraft (Schulz et al. 2000, 2001) indicate that, at rotational phases 0.33 and 0.77, the luminosity of θ^1 Ori C is $2.0 \times 10^{32} \text{ erg s}^{-1}$ [for a hydrogen column density towards the star of $(1.9 \pm 0.3) \times 10^{21} \text{ cm}^{-2}$]. This is more than twice as small as the earlier (and presumably less accurate) estimate of $4.6 \times 10^{32} \text{ erg s}^{-1}$ derived by Gagné et al. (1997) from observations with the High-Resolution Imager (HRI) aboard *ROSAT*, around the phase of minimum H α emission (i.e. phase 0.5), and assuming an interstellar column density of $3 \times 10^{21} \text{ cm}^{-2}$. The resulting fits to the *Chandra* spectra indicate that the X-ray radiation includes a dominant soft component around 0.8 keV (in agreement with the earlier results from the *ROSAT* all-sky survey, Berghöfer, Schmitt & Cassinelli 1996), as well as an additional hard component at 3.2 keV contributing only 7 per cent to the total flux (Schulz et al. 2001).

From a preliminary analysis of the strengths of individual X-ray lines, Schulz et al. (2000) conclude that these X-rays come from confined, hot and dense regions, with volume emission measures ranging between 1.5×10^{54} and $2.5 \times 10^{56} \text{ cm}^{-3}$ and electron densities above 10^{12} cm^{-3} . Moreover, Schulz et al. (2000) obtain that the mean width of these X-ray spectral lines is of the order of 800 km s^{-1} , which is much smaller than the terminal velocity in the wind of θ^1 Ori C. All this argues strongly in favour of the X-ray emission being produced in regions where the O star wind is still slow and dense (i.e. within a few stellar radii of the hot-star surface). Additionally, it indicates that this X-ray radiation is intrinsic to the hot star and not related to its binary nature.

The X-ray flux received from θ^1 Ori C over the 0.1–2.0 keV energy range is known to vary with rotational phase, with a flat minimum about the phase of minimum H α emission (ranging from phases 0.25 to 0.75 and during which both *Chandra* observations reported above were recorded) and a maximum at phase 0.0 (corresponding to maximum H α emission) at which θ^1 Ori C is about 40 per cent brighter than at the X-ray minimum (Caillaud et al. 1994; Gagné et al. 1997). No information is yet available on how the actual X-ray continuum or spectral lines vary with

rotational phase at different wavelengths. The observed rotational modulation of the X-ray radiation received from θ^1 Ori C further demonstrates that the corresponding emission is intrinsic to the O star itself and not attributable to the presence of a companion.

4 MAGNETIC MODELLING

We assume in the following that θ^1 Ori C hosts a rather simple, approximately dipolar, large-scale magnetic field, the axis of symmetry of which is tilted with respect to the rotation axis (the oblique rotator model of Stibbs 1950). This field structure is described by two parameters, its polar strength B_p and its obliquity angle β with respect to the rotation axis.

There are two possible ways of modelling the spectropolarimetric data. The most conventional method consists in measuring and adjusting the phase dependence of low-order moments of the detected Stokes V profiles, as done by Borra & Landstreet (1980) or Mathys (1991) in the particular case of CP stars; the other involves a straight fit to the Stokes V data (e.g. Piskunov 1985). While only the latter can be used for very complex field structures such as those of cool active stars (e.g. Donati & Cameron 1997), both are found to give valuable and complementary results when the field features a simple large-scale structure (e.g. Donati et al. 2001).

4.1 Modelling the longitudinal field curve

Very accurate longitudinal field estimates B_{ℓ} can be easily obtained by measuring the first moment of the Stokes V profile (normalized by the line equivalent width), as detailed by Donati et al. (1997) and Wade et al. (2000). The B_{ℓ} values and error bars we derive from the five mean LSD Stokes V profiles obtained in Section 2 (using an integration window of 76 km s^{-1} on both sides of the line centre) are equal to $357 \pm 46 \text{ G}$, $37 \pm 35 \text{ G}$, $257 \pm 49 \text{ G}$, $191 \pm 63 \text{ G}$ and $257 \pm 73 \text{ G}$, respectively, for rotational phases of 0.033, 0.621, 0.789, 0.920 and 0.177. A cosine fit to these points (see Fig. 2) yields a reduced χ^2 of 1.03, a phase shift between maximum longitudinal field and maximum H α emission (i.e. phase 0.0) of 0.01 ± 0.05 as well as a longitudinal field semi-amplitude B_{max} of $160 \pm 35 \text{ G}$ about a mean value B_0 of $172 \pm 30 \text{ G}$.

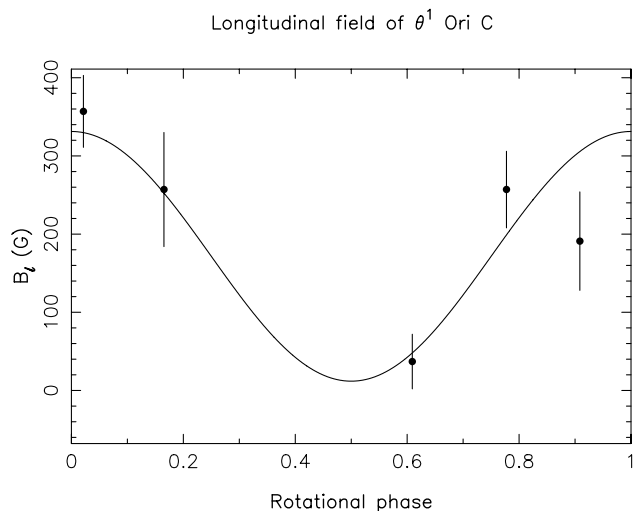


Figure 2. Longitudinal field estimates (filled circles) and error bars derived from our five mean LSD Stokes profiles, as a function of rotational phase (using the ephemeris of Stahl 1998). The full line depicts the least-squares cosine fit to the data.

For a tilted dipole, the variation of B_ℓ with rotation phase ϕ is given by Preston's (1967) well-known relation:

$$B_\ell = B_p \frac{15 + u}{20(3 - u)} [\cos \beta \cos i + \sin \beta \sin i \cos 2\pi(\phi - \phi_0)],$$

where u denotes the continuum limb darkening parameter at the wavelength of the measurements (equal to $u = 0.16$ in the particular case of θ^1 Ori C) and ϕ_0 the phase of maximum longitudinal field. A quantitative estimate of β (as a function of i) can be derived by measuring the ratio of the longitudinal field minimum to the longitudinal field maximum, equal to $\cos(\beta + i)/\cos(\beta - i)$ according to the previous formula. From the fit to our five B_ℓ values, we obtain that this ratio is 0.04 ± 0.15 , implying that $\beta + i$ is equal to 87° , within less than 10° . We thus derive that B_p is 1240 ± 170 G if i is close to 45° , and as much as 1570 ± 220 G and 1660 ± 230 G if i reaches 25° or 65° , respectively.

We also find that phases of maximum longitudinal field (for which the magnetic axis comes closest to the line of sight) coincide with phases of maximum emission in UV and optical wind lines (i.e. phase 0.0, Stahl et al. 1996), while phases of zero longitudinal field (for which the magnetic axis is perpendicular to the line of sight) correspond to phases of maximum absorption in UV wind lines, within about 5 per cent of the rotation cycle. It therefore strengthens the parallel between θ^1 Ori C and hot magnetic CP (e.g. Shore & Brown 1990) and non-CP (Henrichs et al. 2002; Donati et al. 2001) for which such phenomenology is observed (e.g. Smith & Groote 2001).

Another conclusion is that the magnetic geometry proposed for θ^1 Ori C by Stahl et al. (1996) and recently rediscussed by Reiners et al. (2000), for which the magnetic axis is supposed to come closest to the line of sight at phase 0.5, is contradicted by our observations.

4.2 Modelling the Stokes V profiles

The second method of deriving constraints on the magnetic field geometry consists of fitting the mean Stokes V LSD profiles directly rather than their first moment only.

The first thing we need in this aim is a description of the local line profile. To reproduce the shape of photospheric spectral lines, Stahl et al. (1996) and Donati & Wade (1999) both had to invoke additional intrinsic line broadening with a Doppler width of as much as about 40 km s^{-1} . Although the physical nature of this line broadening term is as yet unknown, it is found to be nevertheless rather common in O and B stars (e.g. Howarth et al. 1997) and could be a direct consequence of the strong wind at the photospheric level. We assume here that the intrinsic profile is a simple Gaussian with a Doppler width of 38 km s^{-1} and a relative central depth (with respect to the continuum level) varying between 10.5 and 13 per cent depending on the rotational phase. Once convolved with a rotation profile with $v \sin i = 20 \text{ km s}^{-1}$, this simple model is found to produce an acceptable fit to the observed mean LSD Stokes I profiles and their equivalent width variation with time (the profiles being deeper around phase 0.0; Stahl et al. 1996; Reiners et al. 2000). The mean wavelength and Landé factor of this model intrinsic profile are set to the values obtained in Section 2 (i.e. 570 nm and 1.085, respectively).

In a second step, we produce model LSD Stokes V profiles at the same phases as our observations, for a large sample of magnetic models corresponding to different polar field strengths B_p (ranging between 0 and 2000 G) and different values of the angle β between the magnetic and rotation axis (ranging between -20° and 100°). Note that we assume for all models that the magnetic axis is closest to the line of sight at phase 0.0. We then quantify how well each model reproduces the observations by computing the corresponding reduced χ^2 value. The results are shown in Figs 3 and 4 for different values of the angle i between the rotation axis and the line of sight.

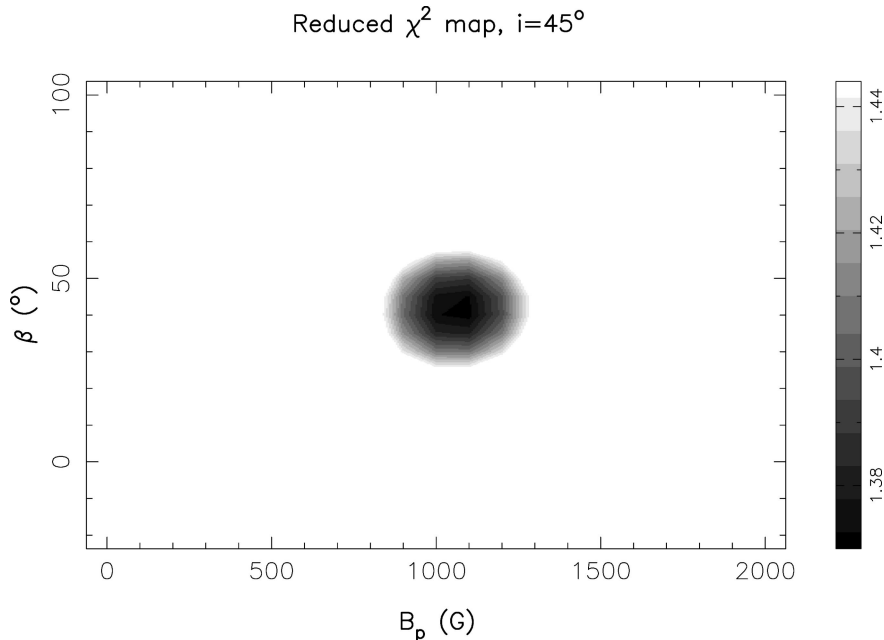


Figure 3. Reduced χ^2 as a function of the magnetic dipole model parameters B_p and β , for an assumed inclination angle i of 45° . The three darkest grey levels correspond to models within the 68 per cent confidence interval, while white areas represent models that can be rejected with a confidence level of better than 99 per cent.

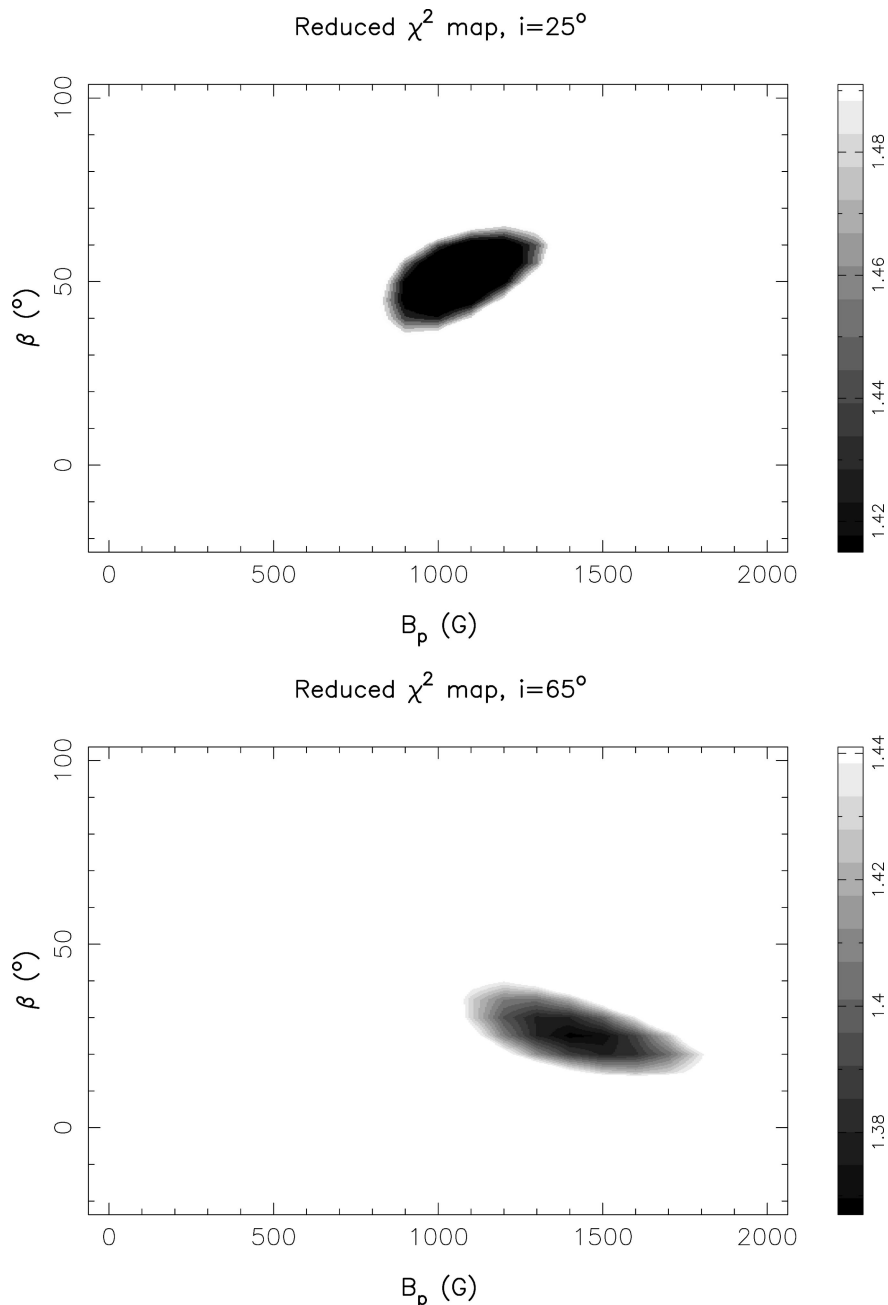


Figure 4. Same as in Fig. 3 for an inclination angle i of 25° (top panel) and 65° (bottom panel).

We obtain that $B_p = 1060 \pm 90$ G and $\beta = 42^\circ \pm 6^\circ$ if i equals 45° , that $B_p = 1070 \pm 100$ G and $\beta = 51^\circ \pm 6^\circ$ if i is as low as 25° and that $B_p = 1420 \pm 150$ G and $\beta = 27^\circ \pm 6^\circ$ if i reaches 65° . All of these estimates are in good agreement with those obtained in Section 4.1, the largest discrepancy (a 2σ difference in B_p) being found in the case with the smallest inclination angle. The resulting fit to the Stokes V LSD profiles is depicted in Fig. 5 in the particular case of $i = 45^\circ$. The smallest χ^2 value achieved for each map ranges between 1.37 and 1.42 (depending on the value of i), showing that the data can almost be fitted down to the noise level. Assuming more complex (though still relatively simple) magnetic models (involving, in particular, an additional quadrupole or octopole component with the same symmetry axis as the dipole component) does not improve the situation significantly,

suggesting that the residual discrepancy with the observed polarization profiles is probably caused by a small underestimate (of the order of 20 per cent) of the error bars.

We therefore confirm the conclusion obtained with the previous technique, i.e. that the magnetic geometry suggested by Stahl et al. (1996) for θ^1 Ori C is contradicted by our observations.

5 MAGNETIC WIND CONFINEMENT

The field we detected at the surface of θ^1 Ori C is undoubtedly strong enough to impact significantly on the radiatively driven stellar wind and even on the whole circumstellar environment. Given the new magnetic geometry we derived in Section 4, we can already conclude that maximum CIV absorption (occurring at

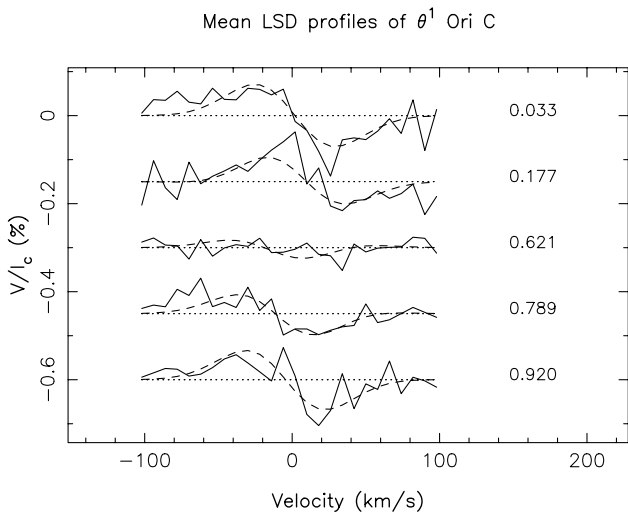


Figure 5. LSD Stokes V profiles of θ^1 Ori C at the five different phases of observations, along with the dipole model that produces the best fit to the data (corresponding to $B_p = 1050$ G and $\beta = 42^\circ$) assuming $i = 45^\circ$. Note that successive profiles are shifted downwards for clarity.

phase 0.5; Stahl et al. 1996) takes place when the magnetic equator appears edge-on to the observer, implying that high-density plasma is trapped in the magnetospheric equator of θ^1 Ori C and forced to corotate with the star as in most He peculiar stars (e.g. Smith & Groote 2001).

One aim of the present study is to see whether the most recent theoretical model of magnetic wind confinement (Babel & Montmerle 1997a) can reproduce quantitatively the extensive observational material available for θ^1 Ori C in the literature. A first attempt in this direction was proposed by Babel & Montmerle (1997b) with the specific aim of reproducing both the X-ray flux of θ^1 Ori C and its modulation with rotational phase. However, the magnetic geometry they assumed for θ^1 Ori C in their work was that suggested by Stahl et al. (1996), which we now know is wrong. Using the magnetic topology derived in Section 4 as a starting point, we derive herein a new magnetospheric model for θ^1 Ori C within the framework of the MCWS model of Babel & Montmerle (1997a).

In the following, we use for θ^1 Ori C the same wind model as that of Babel & Montmerle (1997b), characterized by a mass-loss rate of $3 \times 10^{-7} M_\odot \text{ yr}^{-1}$ (for a spherically symmetric wind) and a terminal velocity of 2500 km s^{-1} (in reasonable agreement with the wind parameters selected in Section 3). Given the uncertainty on \dot{M} , we also consider two additional values for this parameter (5 times larger and smaller than the standard one) to check the impact on our modelling. We finally assume that the magnetic field of θ^1 Ori C is a 1.1-kG dipole inclined at 42° with respect to the rotation axis, in agreement with the results derived in Section 4 for the most probable value of the inclination angle $i = 45^\circ$.

5.1 Standard MCWS model

As briefly mentioned above, the basis of the MCWS model of Babel & Montmerle (1997a) is that a dipolar magnetic field confines and redirects the stellar wind streams from both magnetic hemispheres towards the magnetic equatorial plane, where their collision produces a strong shock. While this shock originally occurs in the magnetic equatorial plane, material accumulation forces it to recede towards the stellar surface until the post-shock

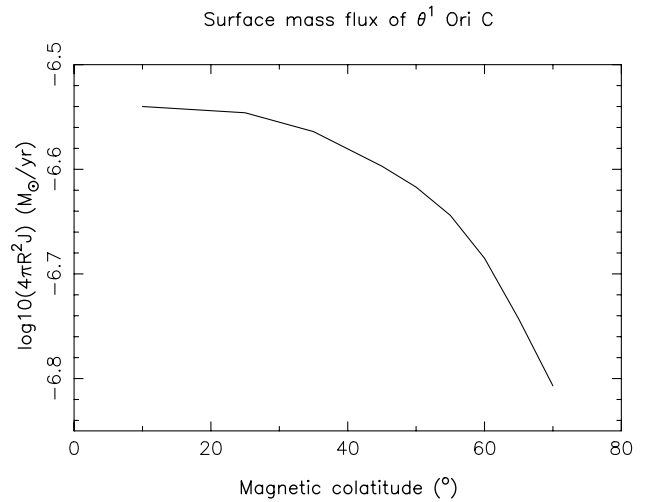


Figure 6. Logarithmic mass flux (multiplied by $4\pi R_*^2$, i.e. normalized to the total stellar surface) as a function of magnetic colatitude at the surface of θ^1 Ori C (for the standard value of \dot{M}). The derived mass-loss rate is equal to that in the non-magnetic (i.e. spherically symmetric) case at the magnetic pole only, and decreases for increasing magnetic colatitudes.

region is sufficiently extended so as to allow dissipation of the energy deposited by the wind (and thus reach a steady state). The resulting circumstellar structure following the shock consists of an extended high-temperature, low-density post-shock region (where X-rays are produced very efficiently) and a geometrically thin, low-temperature, high-density ‘cooling disc’ located in the magnetic equatorial plane.

In the standard MCWS picture, one makes the crude assumption that the field lines are not affected by the wind flow; one can thus derive wind solutions at various magnetic colatitudes by simply solving the momentum equation along the field lines (the divergence of field lines being taken into account through the continuity equation). This assumption implies, in particular, that the wind is no longer spherically symmetric, with a surface mass flux being a function of magnetic colatitude (see Fig. 6). This picture is of course only valid up to the point where the magnetic pressure in the magnetosphere exceeds the wind ram pressure, i.e. for distances smaller than the Alfvén radius R_A . For simplicity, we consider here that the wind is totally confined by the magnetic field within the volume including all field lines intersecting the magnetic equator at a distance smaller than the Alfvén radius. We call this volume the ‘closed magnetosphere’ in the following.

We further assume that in the rest of the circumstellar volume (called the ‘open magnetosphere’), the wind is no longer magnetically controlled and quickly returns to being spherical symmetry. In this basic picture, the post-shock region is thus totally confined to the closed magnetosphere. Note that this is of course a simplifying assumption; we indeed expect the wind in the open magnetosphere (and, in particular, just outside of R_A) to be affected by the magnetic field and even to be potentially redirected towards the magnetic equator, as described for instance in Babel & Montmerle (1997b). However, the closed magnetosphere of θ^1 Ori C should be rather large owing to the strength of the magnetic field (much larger, in particular, than initially predicted by Babel & Montmerle 1997b), implying that the open magnetosphere should only play a marginal role in explaining most of what we observe on θ^1 Ori C. We therefore neglect it in this study. Given the magnetic field estimate obtained in Section 4, we obtain that the Alfvén radius of θ^1 Ori C in the wind itself is located at a distance of about

$3R_*$ from the centre of the star for the standard \dot{M} . However, one actually expects the wind to start distorting the field lines before the ram pressure equals the magnetic pressure. To examine how much this effect modifies the results, we computed several models with different values of R_A .

The temperature and density structures of the closed magnetosphere that we derive within the framework of this simple model (and for standard mass loss) are shown in Fig. 7. In particular, we observe that temperatures in excess of 10 MK (and locally as large as 30 MK) are reached in the post-shock region simultaneously with H number densities of about 10^{10} – 10^{11} cm^{-3} , a value normally restricted to regions within $0.2R_*$ of the stellar surface in conventional non-magnetic wind and wind-shock models. This corresponds rather well with the temperatures derived by Schulz et al. (2000) from new *Chandra* spectra of θ^1 Ori C. The densities they obtain from fitting He-like X-ray triplets (well above 10^{12} cm^{-3}) are, however, significantly larger than those we derive;

this is most probably the result of the fact that Schulz et al. (2000) did not take into account the effect of the strong stellar UV radiation (and thus the radiative excitations they induce on the He-like triplets), leading to overestimates of the density by as much as a few orders of magnitudes (e.g. Waldron & Cassinelli 2001). In this context, the measurements of Schulz et al. (2000) can only be viewed as upper limits.

We also find that the ram pressure just before the shock reaches a maximum of about $140 \text{ g cm}^{-1} \text{ s}^{-2}$ for field lines with colatitudes of 45° – 50° , and decreases for both higher and lower field line colatitudes (down to about 120 and $110 \text{ g cm}^{-1} \text{ s}^{-2}$ for 35° and 60° , respectively). The total (i.e. thermal plus ram) pressure in the post-shock region (equal to the pre-shock wind ram pressure at the shock front) also decreases as we move outwards along the field lines. Close to the magnetic equator, this total pressure reaches a maximum value of about $110 \text{ g cm}^{-1} \text{ s}^{-2}$ at a distance of $1.5R_*$ from the centre of the star (magnetic colatitude of the field line

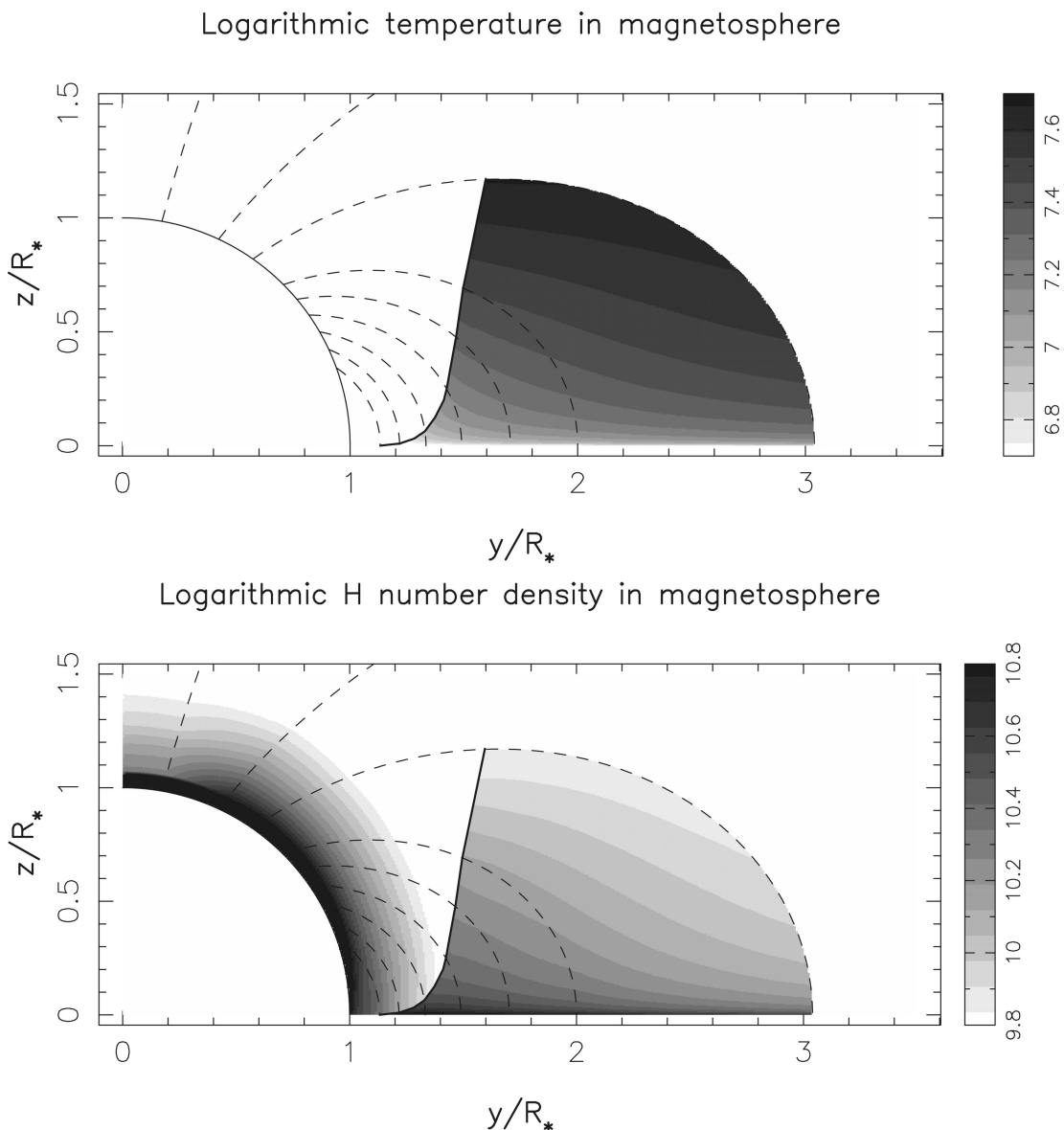


Figure 7. Logarithmic temperature (top panel) and H number density (bottom panel) in the magnetosphere of θ^1 Ori C, assuming standard mass loss and an Alfvén radius of $3R_*$. The thick line depicts the location of the shock, while the dashed ones illustrate the field lines corresponding to footpoint colatitudes of 70° , 65° , 60° , 55° , 50° , 45° , 35° , 25° and 10° .

Table 2. Disc density ρ_D and thickness h_D as a function of radius, for a standard mass-loss rate (columns 2 and 3) or a mass-loss rate 5 times smaller than the standard value (columns 4 and 5). A disc temperature of 40 000 K was assumed in both cases.

r (R_*)	Standard \dot{M}		$5 \times$ reduced \dot{M}	
	ρ_D (10^{12} cm^{-3})	h_D (R_*)	ρ_D (10^{12} cm^{-3})	h_D (R_*)
1.1	5.0	0.021	1.0	0.004
1.2	7.6	0.055	1.5	0.011
1.3	9.5	0.052	1.9	0.025
1.5	10.1	0.031	2.0	0.060
1.7	10.0	0.018	2.0	0.090
2.0	9.4	0.010	1.9	0.050
2.5	8.5	0.005	1.7	0.023
3.0	7.6	0.002	1.5	0.012

footpoint of 55°) and decreases down to about $80 \text{ g cm}^{-1} \text{ s}^{-2}$ at distances of 1.22 and $3.0 R_*$ (magnetic colatitude of the field line footpoint of 65° and 35° , respectively). This requires the density of the cooling disc ρ_D to be equal to about 10^{13} cm^{-3} if we assume a disc temperature of about 40 000 K.

The geometry of the derived models depends only weakly on the assumed mass-loss rate. Smaller \dot{M} values produce slightly lower temperatures in the post-shock region (by about 25 per cent for a factor of 5 in mass-loss rate), with the shock front now being located closer to the stellar surface. It means, in particular, that all densities and pressures in the wind, post-shock region and cooling disc scale roughly linearly with the assumed mass-loss rate.

5.2 Disc properties

The above assumptions also imply that all wind plasma within the closed magnetosphere ends up piling up in the magnetic equator, forming the so-called cooling disc. Being forced to corotate with the field, the ionized disc plasma experiences a non-zero local effective gravity g_{eff} (defined as the gravitation plus centrifugal acceleration) and is therefore dynamically unstable. As described in Donati et al. (2001) in the particular case of β Cep, two different types of instabilities can develop in the disc, depending essentially on the strength of the local magnetic field. If the field is strong enough, the disc plasma transfers its weight back on to the wind and eventually leaks towards the star along field lines. If not, field lines become more and more distorted in an attempt to resist the ever increasing effective gravitational force, until they reconnect and dump the disc plasma back on to the stellar surface. In both cases, the plasma blown by the wind within the closed magnetosphere ends up going back to the star, producing some kind of large-scale circulation.

In θ^1 Ori C, we find that the limit between both regimes occurs roughly at a distance of about $R_d = 1.3 R_*$, from the centre of the star for a standard mass loss (1.1 and $1.7 R_*$, respectively, for \dot{M} values 5 times larger and smaller). Within this limit, the disc plasma is regularly transferred back to the star along the magnetic field lines. The maximum thickness h_D that the disc reaches in this area ranges from about 0.02–0.05 R_* between $1.1 R_*$ and R_d for a normal mass-loss rate, and from 0.005 to 0.09 R_* when \dot{M} is reduced by a factor of 5. At distances larger than R_d , the portion of field lines that crosses the magnetospheric equator starts to become significantly distorted no more than about 1–2 d after the initial shock; at this time, h_D decreases from about 0.05 to 0.002 R_* as one goes from 1.3 to $3.0 R_*$ from the centre of the star. Both the disc

filling times (defined as the time during which field lines manage to hold the disc material with no significant distortion, see Donati et al. 2001) and the disc thicknesses outside R_d (and estimated at disc filling times) are found to scale up roughly linearly with the inverse of \dot{M} . This implies, in particular, that the column densities across the disc at disc filling times should be roughly independent of \dot{M} at any given radius between R_d and R_A , ranging from about 10^{22} cm^{-2} at $3 R_*$ up to a few 10^{23} cm^{-2} at $1.3 R_*$. The disc profile as predicted by MCWS at disc filling times is listed in Table 2 for both a standard mass-loss rate and a mass-loss rate 5 times smaller than the standard value.

Assuming that the disc continues to thicken at constant density after disc filling times, we find that most of the plasma piling up in the magnetospheric equator returns back to the star through quasi-static field line distortion within no longer than 15 d (at a distance of $1.3 R_*$) to 60 d (at $2 R_*$), for standard mass loss. It also implies that the disc never exceeds a total thickness of about $0.4 R_*$. Using a mass-loss rate reduced by a factor of 5 we also obtain the same order of circulation time-scale, with a maximum disc thickness of the order of $0.7 R_*$. Given the current sheet that develops in the magnetic equatorial plane as the disc collapses, we actually expect rapid reconnection to occur and therefore to keep both the plasma circulation time-scale and the disc thickness well within their maximum values, and probably not far from their minimum values (respectively, equal to the disc filling time and the disc thickness at disc filling time, as defined above).

If our interpretation of the Be episodes of β Cep is correct, it automatically implies that θ^1 Ori C should also undergo similar outbursts. However, although the rate of mass input in the magnetosphere is 300 times larger for θ^1 Ori C than for β Cep, the time-span during which plasma accumulates in the disc before it goes back to the star is also about 300 times shorter; the Be episodes of θ^1 Ori C should therefore be roughly as energetic as those of β Cep, but should show up much more weakly in spectroscopic observations given that θ^1 Ori C is about 10 times intrinsically brighter than β Cep. The H α spectroscopic signatures of the Be episodes, the equivalent width of which peaks at 0.1 nm in β Cep, are thus expected to reach an equivalent width of the order of 0.01 nm in θ^1 Ori C, and could thus easily be masked by the intrinsic H α variability of this star (the total amplitude of which is about 0.3 nm with a dispersion of a few 0.01 nm; Stahl et al. 1996).

Another possibility is that the cooling disc continuously leaks outwards, rather than retaining the wind plasma. Although in this study we have assumed that field lines (at least up to $2\text{--}3 R_*$) were not distorted by the wind, they may actually open outwards slightly under the wind ram pressure, implying that the plasma flowing from the post-shock region reaches the magnetospheric equator with a non-zero outward radial velocity. Although this could be the fate of the plasma in the outer limit of the closed magnetosphere, we consider this option to be fairly unlikely for the bulk of the closed magnetosphere. Indeed, the amount of gravitational energy that the disc plasma has to counteract to be able to escape freely corresponds to velocities in excess of 1000 km s^{-1} , which is much higher than what the plasma is left with after the shock.

Even though we estimate that this second possibility is fairly improbable, we nevertheless consider two scenarios in the following, one where a dense cooling disc forms in the magnetospheric equator, and another one where most material reaching the equator is rapidly expelled outwards by some as yet unclear mechanism with no cooling disc (or only a very thin one) forming in the magnetospheric equator.

6 SPECTRAL PREDICTIONS

To investigate in detail the validity of our work, we need to check whether the level and rotational modulation our model predicts for various magnetospheric spectral indicators (e.g. fluxes, line profiles and polarization at different wavelengths) agree with the observations of θ^1 Ori C published in the literature. If our picture is correct, most of these indicators should indeed undergo some amount of rotational modulation as a result of the variable viewing angle (defined as the angle between the magnetic axis and the line of sight) under which the magnetosphere appears to the observer as the star rotates. We focus in this first study on two main families of indicators, the X-ray fluxes and line profiles, and the optical/UV wind lines.

6.1 X-ray fluxes

As recalled in Section 3 already, θ^1 Ori C produces stronger-than-average X-ray radiation that varies significantly with rotation phase. In the context of our model, this modulation could be the result of three different factors: the obscuration of the X-ray-emitting post-shock region by the star itself; the eclipse by the cooling disc (if present); or absorption by the cool wind surrounding the closed magnetosphere. To check whether our description is plausible and to help discriminate between the various parameters we have introduced, we consider here several variations of our model, with and without a cooling disc opaque to X-rays, and with a closed magnetosphere extending to either 2 or $3 R_*$. To examine the impact of the X-ray-absorbing cool wind surrounding the post-shock region, we further consider an additional toy model in which the wind absorption is ignored. We also investigate the consequence of varying the mass-loss rate, within the limits mentioned in Section 5. Altogether, we consider six different models, the parameters of which are summarized in Table 3.

To quantify the X-ray emission produced in the post-shock region of our models, we compute, for all points of the magnetosphere, the local X-ray emissivity from MeKaL models (Mewe, Kaastra & Liedahl 1995) in the energy range 0.1–10 keV. Given the minimum column density across the disc of about 10^{22} cm^{-2} , we obtain that the disc is essentially opaque to X-rays in most of the 0.2–2.0 keV energy band. Note that we further assume that the opaque disc (if present) extends from the stellar surface to far enough beyond the Alfvén radius to ensure that only half the magnetosphere of θ^1 Ori C is visible to the observer at any

Table 3. Parameters of the various models considered in Section 6. The second column lists the assumed Alfvén radius R_A , the third one the mass-loss rate (in units of the standard mass-loss rate, see Section 3). The last two columns indicate whether a cooling disc opaque to X-rays and the absorption by the surrounding cool wind are taken into account in the computations.

Model number	R_A (R_*)	\dot{M}	Disc	Wind abs.
1	2	$\times 1$	yes	yes
2	2	$\times 1$	yes	no
3	2	$\times 1$	no	no
4	3	$\times 1$	yes	no
5	3	$\times 0.2$	yes	yes
6	2	$\times 5$	yes	yes

given time, even for viewing angles (defined as the angle between the line of sight and the magnetic axis) as large as 87° .¹ The absorption by the surrounding magnetosphere (whenever taken into account) is computed on a 100×100 point grid, using the cross-sections from Morrison & MacCammon (1983) and taking H and He as fully ionized. We also take into account the absorption by the wind outside the Alfvén sphere (assumed to be spherically symmetric) as well as by the interstellar neutral H along the line of sight, for which we adopt a global column density value of about $2 \times 10^{21} \text{ cm}^{-2}$ (Schulz et al. 2001). We finally carry out the integration of the radiative transfer for various viewing angles and convolve the theoretical X-ray spectrum with the response of the *ROSAT* HRI instrument.

Given our assumptions on the (opaque) disc, the eclipse it produces simply amounts to halving the X-ray flux towards the observer independently of the rotation phase. Only the other two factors, i.e. the obscuration by the central star and the absorption by the surrounding cool wind, are thus expected to induce rotational modulation of the X-ray flux from θ^1 Ori C. Both effects should not produce the same signatures, however; while the eclipse by the central star should obscure the largest fraction of X-ray photons when the magnetosphere is seen edge-on (i.e. at phase 0.5), the absorption by the cool wind should be maximum when the post-shock region is observed through the densest wind regions (at phase 0.0). Moreover, the wind absorption affects mostly the soft part of the spectrum, while the eclipse by the central star is almost achromatic.²

The maximum and minimum X-ray fluxes obtained for our models are listed in Table 4. The first conclusion is that all of our models produce significantly more X-rays than the *ROSAT* HRI observations indicate (i.e. a count rate varying periodically between 0.3 and 0.4 count s^{-1} , Gagné et al. 1997), by a typical factor of about 5 (for models 1 and 2) to more than 10 (for models 3, 4 and 6). Only model 5 (mass loss reduced by a factor of 5) matches the observations within about 50 per cent. Our simulations therefore suggest that the mass-loss rate of θ^1 Ori C is significantly smaller than the theory of radiatively driven stellar winds predicts, and may even be weaker than that assumed for model 5. Moreover, we obtain that models involving either a dense cooling disc (halving the X-ray flux towards the observer), or/and a smaller Alfvén radius (decreasing the volume of the closed magnetosphere for a given polar field and mass loss parameters), provide a better match to the observations and can be considered to be more probable. Another potential explanation is that the wind shock is less efficient than assumed in our simulation, and that a smaller fraction of the wind kinetic energy is changed into X-rays.

The predicted *ROSAT* HRI light curve corresponding to our best models (i.e. 1, 5 and 2) are shown in Fig. 8, once rescaled to match the observations of Gagné et al. (1997). While the amplitude of the synthetic X-ray light curve we obtain for model 2 is roughly

¹ Note that this assumption may not be entirely consistent with the results obtained above, indicating for instance that the disc may be opaque only beyond R_d and within R_A (see Section 5.2); this point is, however, not completely clear, as it depends critically on the actual fate of the plasma piling up in the disc. We therefore preferred to keep the problem as simple as possible and avoid the introduction of additional parameters, at least until more direct constraints are available from observations.

² The stellar eclipse is not totally achromatic though, since the different regions of the spectra do not come from the same spatial regions (harder X-rays being produced in hotter parts of the post-shock region).

Table 4. Maximum/minimum X-ray fluxes emerging from the magnetosphere and towards the observer, obtained for all models included in Table 3. Columns 2–5, respectively, list the total X-ray flux, the X-ray flux in the 0.2–2.0 keV spectral band, the X-ray flux multiplied by the *ROSAT* HRI instrumental efficiency, and the corresponding *ROSAT* HRI count rates.

Model number	L_x (10^{32} erg s $^{-1}$)	L_x (0.2–2.0 keV) (10^{32} erg s $^{-1}$)	L_x (HRI) (10^{32} erg s $^{-1}$)	HRI count rate (count s $^{-1}$)
1	24.0/21.1	20.2/17.5	7.25/5.95	1.75/1.45
2	31.2/24.8	26.6/21.1	9.65/7.65	2.43/1.92
3	62.4/49.6	53.2/42.2	19.3/15.3	4.86/3.84
4	72.4/60.8	56.0/46.7	20.9/17.5	5.09/4.24
5	8.25/6.92	7.08/5.87	2.33/1.93	0.58/0.48
6	144/94.1	116/64.7	43.0/30.9	10.6/6.95

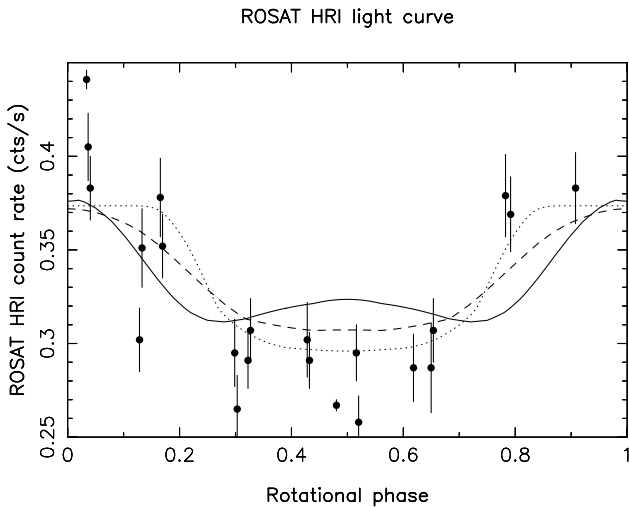


Figure 8. Predicted *ROSAT* HRI light curve corresponding to model 1 (full line), 5 (dashed line) and 2 (dotted line), once rescaled (by respective factors of 0.20, 0.65 and 0.15) to match the observations of Gagné et al. (1997, symbols and error bars).

compatible with the observations, taking into account wind absorption (i.e. model 1) narrows the peak of the light curve (around phase 0.0) and decreases significantly the agreement with the *ROSAT* HRI data (especially around phase 0.8). It suggests again that the wind absorption is weaker than assumed, and therefore, that the mass-loss rate we used is somewhat overestimated. Model 5 (with \dot{M} decreased by a factor of 5) indeed provides better agreement, although the amplitude of the synthetic light curve is still weaker than the observations indicate. This suggests that the bulk of the X-rays we observe suffers stronger obscuration at phase 0.5 than our models predict, and hence comes from a region closer to the stellar surface. Although this should normally imply that the size of the closed magnetosphere we assumed is overestimated, this conclusion is apparently incompatible with the previous one suggesting that the assumed mass-loss rate of θ^1 Ori C is overestimated (a weaker mass-loss rate implying a larger magnetospheric volume for a given field strength and terminal wind velocity). This contradiction is discussed further in Section 6.3.

6.2 X-ray lines

Further progress on this particular issue requires independent confirmation that the assumed mass-loss rate of θ^1 Ori C is indeed

too large. This could be obtained by looking at how the X-ray variability changes with wavelength. This dependence is shown in Fig. 9 for models 5, 1 and 6 (from top to bottom). We obtain that the X-ray light curve at high energies essentially reflects the obscuration by the central star (maximum and minimum flux at phase 0.0 and 0.5, respectively). While this is also the case at low energies for the smallest \dot{M} , the light curve below 1 keV is significantly contaminated, and often completely dominated, by the wind absorption (maximum and minimum flux at phase 0.5 and 0.0, respectively) when \dot{M} is larger than or equal to the standard mass loss. In the intermediate domain (i.e. between 1 and 3 keV roughly) as well as in the *ROSAT* HRI bandwidth (see Fig. 8), both effects are visible simultaneously if \dot{M} is of the order of the standard mass loss, resulting in a more complex rotational modulation with two local maxima (at phase 0.0 and 0.5). The existing *ROSAT* HRI data, although sufficiently accurate to reject unambiguously model 6 (predicting a light curve in complete anticorrelation with the observations), are, however, still too noisy to be able to distinguish between models 1 and 5. By providing colour-dependent light curves similar to those of Fig. 9, future *Chandra*/*XMM* data should thus be able to yield a very strong constraint on the actual mass-loss rate of θ^1 Ori C.

Another way to improve our description of the magnetosphere, and of the cooling disc in particular, is to look at the shape and rotational modulation of specific X-ray lines. In Fig. 10, we simulated dynamic spectra for an arbitrary X-ray line of θ^1 Ori C, when an opaque cooling disc is assumed to be present in the magnetic equator (i.e. model 1, left-hand panel) and when the disc is optically thin to X-rays (i.e. model 3, right-hand panel). We assumed in this case an instrumental resolution of about 1500 (i.e. 200 km s $^{-1}$), comparable with what the most recent X-ray spectrographs (i.e. HETGS aboard *Chandra* and RGS aboard *XMM*) can achieve. While the synthetic profiles we obtain when the disc is seen close to edge-on (i.e. around phase 0.5) are very similar in both cases, they differ rather drastically when the magnetosphere is observed at small viewing angles (around phase 0.0), featuring either a moderately redshifted line (when the cooling disc is indeed opaque) or a double peak profile centred on the stellar radial velocity (if the disc is optically thin to X-rays). By looking at X-ray lines at different wavelengths, we should even be able to bracket the average column density within the cooling disc.

Moreover, by measuring the shift of both peaks (or of the line itself if only one peak is visible) with respect to the nominal line wavelength in the stellar rest frame and comparing it with the value predicted by MCWS (of the order of 140 km s $^{-1}$ for the specific line we used), one could additionally check whether the velocity field MCWS predicts in the post-shock region is correct. We also

obtain that the size of this shift varies with the assumed mass-loss rate, larger and smaller \dot{M} values producing, respectively, stronger and weaker shifts (see Fig. 10, bottom panels). The same effect is also observed among various X-ray lines for a given model, lines with higher excitation energies being formed at higher temperatures (i.e. at larger distances from the disc) and thus featuring larger shifts. The detailed shape of the line profile at phase 0.0 is shown in Fig. 11.

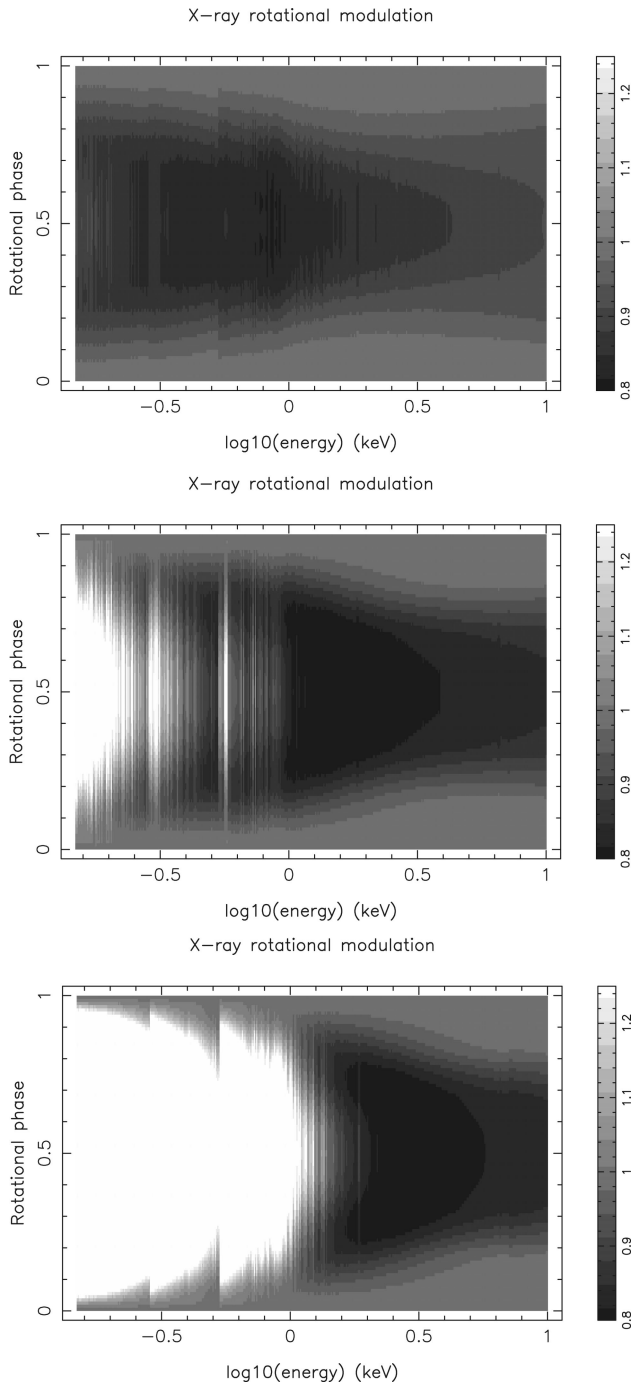


Figure 9. X-ray rotational modulation predicted for θ^1 Ori C by models 5 (top panel), 1 (middle panel) and 6 (bottom panel), in the energy range 0.1–10 keV. All spectra were normalized with respect to that at phase 0.0. Relative X-ray luminosities are depicted by grey levels, with black and white representing, respectively, -20 and $+25$ per cent changes with respect to the flux at phase 0.0.

These predictions can already be compared with the most recent X-ray observations of Schulz et al. (2000) recorded with *Chandra*/HETGS at phases 0.77 and 0.33. Although they mention the presence of lines with Doppler widths in excess of 1000 km s^{-1} (in strong contradiction with our results), it is not clear from their study whether the lines they used are truly single lines. What is clear, however, from their fig. 3 is that the Doppler widths they measure are compatible, for the majority of the spectral features they used, with the instrumental broadening, and should therefore be considered as upper limits. Schulz et al. (2000) also mention that they do not observe any measurable shifts nor asymmetries of spectral line, in agreement with our results for these specific rotational phases (see Fig. 10).

We stress the fact that meaningful comparisons with predictions of the MCWS model can only be achieved from observations of single X-ray lines of θ^1 Ori C, secured at both extreme configurations of the magnetosphere (phase 0.0 and 0.5).

6.3 Optical and UV lines

Another important test of the MCWS we developed for θ^1 Ori C consists in comparing the predicted versus the observed dynamic spectra of lines that are supposed to form mostly within the magnetosphere. As recalled in the introduction, many of these lines are known to exhibit very obvious rotational modulation, both in the optical and UV wavelength domains. The spectral features for which extensive studies are available in the literature are $H\alpha$, the He II line at 468.6 nm, as well as the C IV and Si IV UV lines around 155 and 140 nm, respectively (Stahl et al. 1996). While $H\alpha$ and the He II line show strong emission concentrating around phase 0.0 (magnetosphere viewed pole-on), the C IV and Si IV doublets both present increased absorption down to fairly large velocities (as much as -2500 km s^{-1}) around phase 0.5 (magnetosphere viewed equator-on).

To obtain estimates of how such lines should vary with rotational phase, we used the synthetic temperature, density and velocity maps of the magnetosphere derived from the above modelling as input into the Monte Carlo stellar wind radiative transfer code of Harries (2000). This tool solves iteratively both the statistical equilibrium for the various non-LTE populations of interest at all locations in the maps, as well as the radiative transfer through the magnetosphere and wind (in Sobolev’s approximation) for various viewing angles. We assumed for this simulation that the cooling disc is that predicted for model 1 (listed in columns 2 and 3 of Table 2) or model 5 (columns 4 and 5). We obtain that, in the context of the MCWS model, most $H\alpha$ emission comes from scattering by the cooling disc and very little from the wind. This first result already demonstrates the existence of the disc, and thus represents an important additional confirmation of the MCWS model.

Moreover, we find that reproducing the strong rotational modulation of the $H\alpha$ emission component of θ^1 Ori C requires a specific velocity field in the disc, with velocity gradients of about 4000 km s^{-1} per R_* (e.g. velocity decreasing from about 100 km s^{-1} at the surface of the inner disc down to zero at the magnetospheric equator) oriented along magnetic field lines. While the cooling disc corresponding to model 1 generates far too much $H\alpha$ emission at phase 0.0, that associated with model 5 yields a reasonable match to the observations of Stahl et al. (1996). The resulting dynamic spectrum (see Fig. 12) shows a striking similarity with that obtained by Stahl et al. (1996, their fig. 6). In particular, the agreement with observations is considerably more

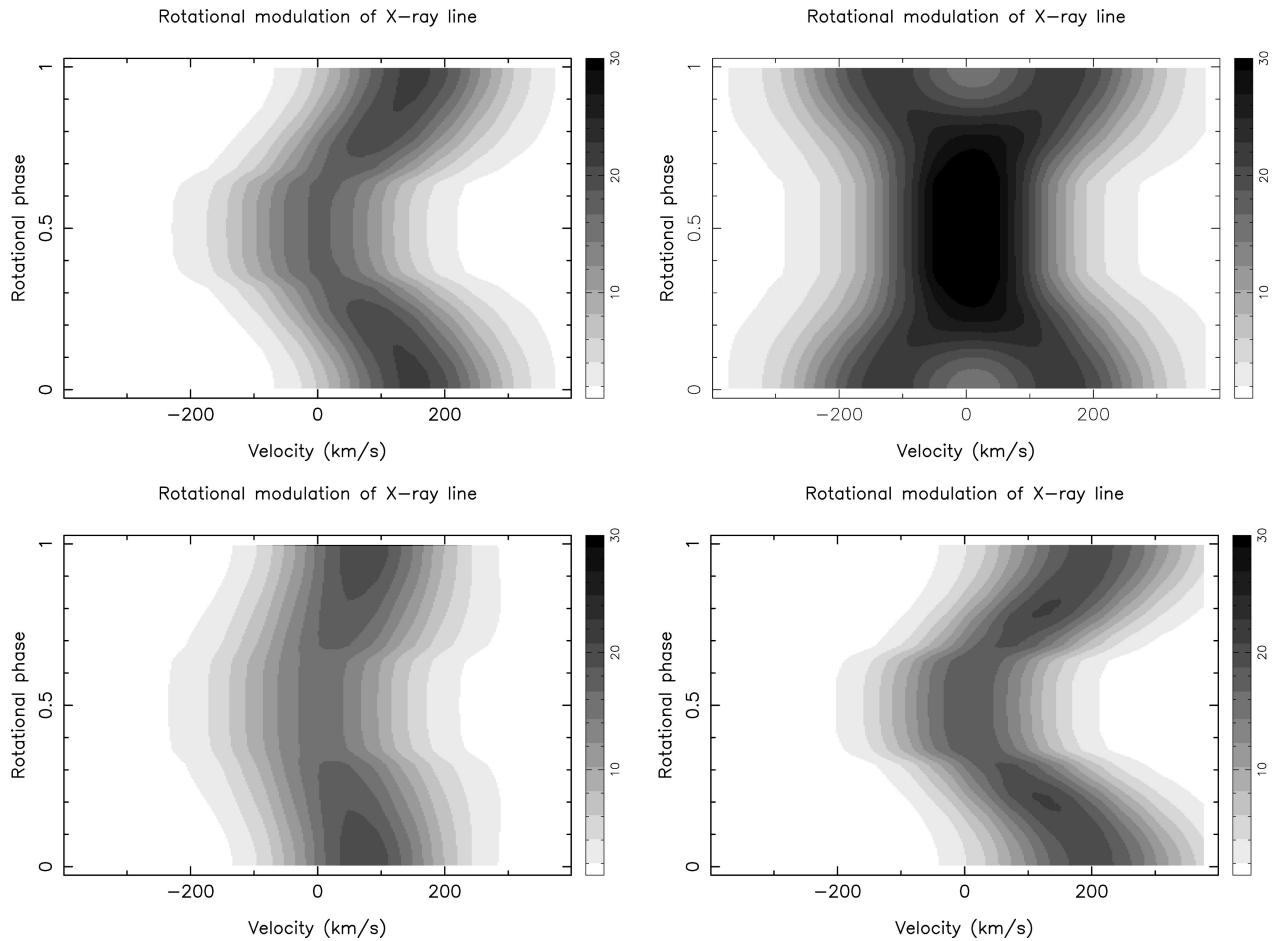


Figure 10. Dynamic spectrum of an arbitrary X-ray line of θ^1 Ori C throughout a complete rotational cycle, as predicted for model 1 (top left-hand panel), model 3 (i.e. top right-hand panel), model 5 (bottom left-hand panel) and model 6 (bottom right-hand panel). Darker grey levels indicate stronger emission.

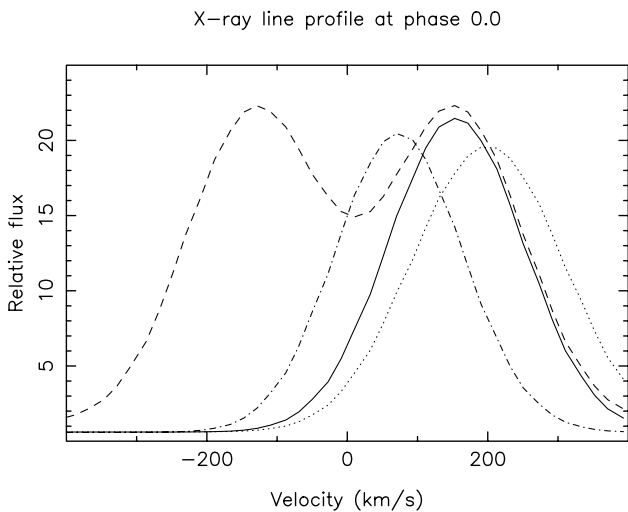


Figure 11. Profile of the X-ray line at phase 0.0 for model 1 (full line), model 3 (dashed line), model 5 (dot-dashed line) and model 6 (dotted line).

convincing than in earlier attempts at modelling the magnetosphere of θ^1 Ori C (e.g. Shore 1999). It suggests that the MCWS concept is supported by the existing $H\alpha$ observations.

However, there are a number of potential problems between the observations and our model. First of all, the velocity field we had to

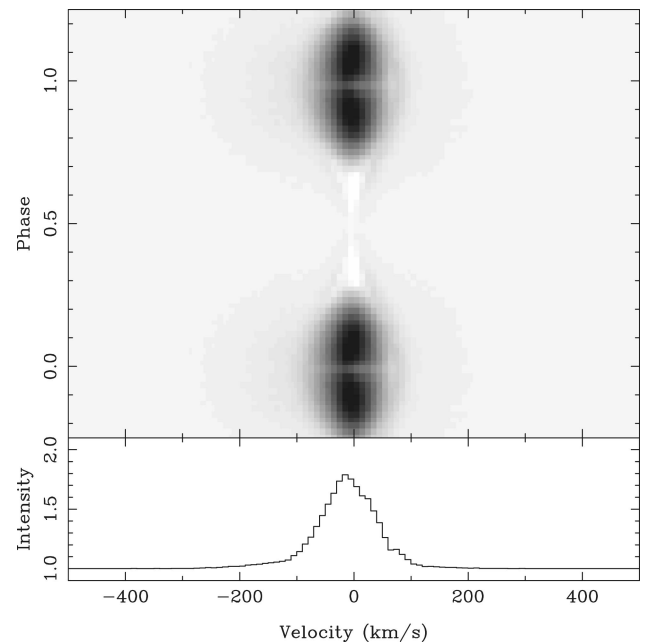


Figure 12. Dynamic spectrum of the $H\alpha$ emission component of θ^1 Ori C as predicted by model 5 (and assuming the disc model in columns 4 and 5 of Table 2). Darker grey levels depict stronger emission. The lower panel shows the synthetic profile obtained at maximum emission (i.e. phase 0.0).

assume in the disc, and without which no proper match to the observed rotational modulation of $H\alpha$ can be obtained, is still rather arbitrary. Although it sounds rather plausible that the disc plasma can either decelerate towards the magnetospheric equator (e.g. for material arriving into the disc) or accelerate towards the star (e.g. for material flowing back to the star along field lines), the exact magnitude of the corresponding velocity gradient is still essentially a matter of speculation. Predicting the exact velocity field in the disc is, however, rather difficult, since it requires the complete two-dimensional (2D) magnetohydrodynamics (MHD) time-dependent problem to be solved consistently, which is far beyond the scope of the present study.

Another apparent difference between our model and the observations is the significant blueshift (of up to 50 km s^{-1}) that the $H\alpha$ spectra of θ^1 Ori C exhibit around phase 0.0 (Stahl et al. 1996), i.e. when the magnetosphere is seen pole on. A closer look also reveals that this blueshift decreases with increasing viewing angle, suggesting that it results from velocities oriented along field lines and directed towards the observer. Although this argues in favour of the velocity field that we had to introduce to match the rotational modulation of the $H\alpha$ line, it also tells us that this velocity field is more complex than the simple velocity gradient we assumed (which, in principle, produces no significant blueshift in the resulting line profile), and may also include a random velocity distribution of turbulent origin (that we cannot easily take into account in our code, based on Sobolev's approximation). Moreover, it also suggests that the bulk of the $H\alpha$ emission is produced within R_d (i.e. where the disc material returns to the star along the field lines, see Section 5.2), therefore supporting a mass-loss rate significantly smaller than the standard one (since R_d increases with decreasing \dot{M}).

The same code can simultaneously compute the level (and rotational modulation) of the continuum polarization (owing mostly to electron scattering in the disc) and the depolarization signature throughout the $H\alpha$ profile that our MCWS model implies. We find that the predicted rate of continuum polarization is maximum when the disc is seen edge-on, peaking at a relative amplitude of 0.3 per cent in the case of model 5. The depolarization signature associated with $H\alpha$ shows a more complex dependence with rotational phase, consequently, of the anticorrelated modulation of the line emission (with a maximum at phase 0.0) and continuum polarization (with a maximum at phase 0.5). The resulting variation is double peaked, with line depolarization signatures reaching a maximum amplitude of about 0.1 per cent at phase 0.25 and 0.75. Although the continuum polarization we predict exceeds the existing observational upper limits slightly (indicating no continuum nor line polarization signatures down to an accuracy of about 0.1 per cent; Oudmajer, private communication), we nevertheless estimate that the discrepancy is rather minor and could possibly be attributed to roughness of the various simplifying assumptions we made; we therefore conclude that our model reproduces grossly the bulk of existing $H\alpha$ observations.

Further tests of our model could be obtained by comparing in a similar way the predictions and observations for other spectral lines formed in the magnetosphere. However, the code we use still assumes that the plasma consists of pure H when solving the non-LTE equations of statistical equilibrium (for the sake of computing speed), and can therefore not be applied to He lines yet. Since the He line at 468.6 nm essentially mimics $H\alpha$, the additional constraints that it brings to the modelling are probably not fundamental. The resonance C IV and Si IV doublets appear to be

much more promising and challenging in that respect. Unfortunately, the code cannot yet properly compute resonance line scattering at the moment. In an attempt to check whether our model could, at least roughly, reproduce the basic features of the observations (enhanced absorption at large velocities towards the observer), we tried to incorporate this possibility into the code, under the simplifying assumption that electron scattering opacity is negligible and using the two-level atom approximation to obtain a rough estimate of the line opacity. In this context, however, we obtain that the C IV absorption is basically phase independent, unless we add some amount of gas within the magnetospheric equator that moves outwards at large velocities.

It therefore suggests that reproducing the variability of these resonance lines requires the inclusion of the open part of the magnetosphere (i.e. beyond R_A) in the model, and, in particular, the corresponding disc component that should precisely feature high-velocity gas in the magnetic equatorial plane moving outwards at velocities approaching the wind terminal velocity (e.g. Babel & Montmerle 1997b). Note that this conclusion appears reasonable given what we know already in the particular case of magnetic CP stars where additional absorption in several UV resonance lines is observed when the magnetosphere is seen edge-on and interpreted as scattering caused by the cool plasma sitting in the magnetospheric equator and forced to corotate with the star (the analogue of our cooling disc, Smith & Groote 2001). The essential difference of θ^1 Ori C with respect to magnetic CP stars is that its mass-loss rate is much larger; we therefore expect to find a larger fraction of the disc material in the open magnetosphere, and thus to observe more absorption at large blueshifts, for θ^1 Ori C than for magnetic CP stars. Although additional work (postponed to forthcoming studies) is of course required to obtain a more quantitative description of what really happens, our arguments suggest that there is no incompatibility between the MCWS model and the existing sets of observations.

7 CONCLUSIONS

We report new spectropolarimetric observations of the very young O star θ^1 Ori C secured in 1999 December and 2000 December with a visitor polarimeter mounted on the Anglo-Australian Telescope and fibre-feeding the high-resolution UCLES spectrograph.

From information available in the literature, we confirm that θ^1 Ori C is most probably of mass $44 \pm 5 M_\odot$ with an age smaller than 0.6 Myr, an effective temperature of $45\,000 \pm 1000 \text{ K}$ and a radius of $8.2 \pm 1.1 R_*$. Given the projected rotation velocity of 20 km s^{-1} and the rotation period of 15.426 d, we find that the inclination angle i of the rotation axis to the line of sight is of the order of $45^\circ \pm 20^\circ$. Both observations and theory indicate that the mass-loss rate of θ^1 Ori C should be of the order of $3 \times 10^{-7} M_\odot \text{ yr}^{-1}$ (assuming a spherically symmetric wind), with a terminal velocity of 2500 km s^{-1} . We also find that, if the radial velocity variations of θ^1 Ori C reported by Stahl et al. (1996) are to be attributed to the presence of the companion recently detected through speckle interferometry (Weigelt et al. 1999), then both stars must possess very eccentric orbits.

Very clear Stokes V signatures are detected in the spectral lines of θ^1 Ori C, and are observed to change shape with the rotation period. This discovery represents the first definite detection of a magnetic field in an O star. We find that these variations can be reproduced convincingly if the star hosts a $1.1 \pm 0.1\text{-kG}$ dipole field, inclined at 42° with respect to the rotation axis (assuming that

the rotation axis is inclined at 45° with respect to the line of sight), with the positive pole coming closest to the observer at phase 0.0. This simple magnetic topology suggests strongly that the field is of fossil origin, establishing simultaneously that θ^1 Ori C is truly a high-mass equivalent of magnetic CP stars, as proposed by Stahl et al. (1996) and Babel & Montmerle (1997b). Additionally, this study also represents the first detection of a fossil field in a very young star.

The magnetic geometry we derive contradicts that predicted by Stahl et al. (1996) and used by Babel & Montmerle (1997b). We carried out a new analysis to see how well the magnetically confined wind-shock model of Babel & Montmerle (1997a) could explain the extensive set of multiwavelength observations available in the literature on θ^1 Ori C. Given the strength of the detected magnetic dipole, we conclude that the radiative wind of θ^1 Ori C is magnetically confined to at least $2R_*$ and probably even further, depending on the exact value of the wind parameters. The collision of the wind streams from both hemispheres generates a strong shock, a very hot and extended post-shock region as well as a cool disc in the magnetospheric equator. We find that the plasma temperature in the post-shock region reaches values in excess of 10 MK, in good agreement with what the new *Chandra* observations of Schulz et al. (2000) indicate. Moreover, the densities we predict, of the order of 10^{10} – 10^{11} cm^{-3} , agree with the upper limits that the incomplete analysis of Schulz et al. (2000) yields. Our model also predicts that the cooling disc should feature a column density of about 10^{22} – 10^{23} cm^{-2} . We predict that the outer disc material should return episodically to the star through both quasi-static field line distortion and rapid reconnection; this though is still a matter of speculation, since no direct evidence exists as yet to test this hypothesis.

In the context of the MCWS model, the rotational modulation of the X-ray flux of θ^1 Ori C can only be interpreted as an eclipse of the post-shock region by the central star (the cooling disc being essentially opaque to X-rays). By trying to match both the observed X-ray flux and X-ray variability, we obtain (assuming that MCWS is correct) that the mass-loss rate predicted for θ^1 Ori C by modern radiatively driven wind models is very likely to be overestimated by as much as a factor of 5 and possibly up to a factor of 10. Fitting the amplitude of the *ROSAT* X-ray light curve requires, in particular, the post-shock region to extend no further than about $3R_*$ – significantly smaller than the volume in which the magnetic pressure dominates the wind ram pressure (the radius of which ranges between 3 and $5R_*$ depending on the assumed mass-loss rate). The exact reason for this discrepancy is not clear as yet, but may be related to the fact that the disc is not completely opaque to X-rays close to the star; by increasing the relative weight of the highly eclipsed portions of the post-shock region in the total X-ray flux and therefore the amplitude of the predicted X-ray light curve, this effect could potentially reconcile both X-ray and magnetic observations.

Investigating what rotational modulation our model predicts for the magnetospheric $\text{H}\alpha$ emission component of θ^1 Ori C is also very instructive. By comparing them with the observations of Stahl et al. (1996), we find, in particular, that most of the emission comes from the cooling disc, thus providing strong evidence for the existence of the cooling disc. We also find that a velocity gradient of the order of 100 km s^{-1} across the cooling disc is necessary to reproduce both the large width and strong rotational modulation of the observed $\text{H}\alpha$ profile. These simulations also argue for θ^1 Ori C having a mass-loss rate at least 5 times smaller than the theoretical predictions. The rough modelling of the C IV UV lines we

performed did not allow us to reproduce the additional absorption observed in the spectrum of θ^1 Ori C at large negative velocities when the magnetosphere is observed edge-on; although a more accurate analysis is needed to confirm this point, we suspect that the disagreement is mostly a result of the fact that the open magnetosphere is neglected in this study.

We therefore conclude that the MCWS model includes most of the physics required to obtain a satisfactory level of agreement with the extensive set of observations available on θ^1 Ori C in the literature. However, we should be able to go even further and pin down most of the parameters that are critical (and, in particular, the mass-loss rate and the average column density across the disc) for a detailed comparison between the model predictions and the observations. We show that new X-ray spectroscopic observations of θ^1 Ori C with either *XMM* or *Chandra* throughout the rotation cycle (and at the very least around phase 0.0 and 0.5) should allow us to make considerable progress on these specific issues, and more generally on the magnetically confined winds of the hot star. Ultimately, one needs to carry out a 2D time-dependent MHD simulation of the whole magnetosphere and wind in order to model all components consistently and understand the fate of the disc material.

ACKNOWLEDGMENTS

We thank R. Oudmaijer for sending us polarimetric observations of θ^1 Ori C prior to publication. We are also grateful to the referee, G. Mathys, for pointing out several errors in an earlier version of the manuscript, as well as to M. Smith for his careful reading of the paper and very valuable comments.

REFERENCES

- Babel J., Montmerle T., 1997a, *A&A*, 323, 121
 Babel J., Montmerle T., 1997b, *ApJ*, 485, L29
 Berghöfer T. W., Schmitt J. H. M. M., Cassinelli J. P., 1996, *A&AS*, 118, 481
 Bernasconi P. A., Maeder A., 1996, *A&A*, 307, 829
 Bessel M. S., Castelli F., Plez B., 1998, *A&A*, 333, 231
 Borra E. F., Landstreet J. D., 1980, *ApJS*, 42, 421
 Brown A. G. A., de Geus E. J., de Zeeuw P. T., 1994, *A&A*, 289, 101
 Caillault J.-P., Gagné M., Stauffer J. R., 1994, *ApJ*, 432, 386
 Cohen D. H., Finley J. P., Cassinelli J. P., 2002, *ApJ*, in press
 Conti P. S., 1972, *ApJ*, 174, L79
 de Zeeuw P. T., Hoogerwerf R., de Bruijne J. H. J., 1999, *ApJ*, 117, 354
 Donati J.-F., Cameron A. C., 1997, *MNRAS*, 291, 1
 Donati J.-F., Wade G. A., 1999, *A&A*, 341, 216
 Donati J.-F., Semel M., Carter B., Rees D. E., Cameron A. C., 1997, *MNRAS*, 291, 658
 Donati J.-F., Wade G. A., Babel J., Henrichs H. F., de Jong J. A., Harries T. J., 2001, *MNRAS*, 326, 1265
 Donati J.-F., Hussain G. A. J., Cameron A. C., Semel M., López Ariste A., Carter B. D., Mengel M., Rees D. E., 2002, *MNRAS*, submitted
 Feldmeier A., 1995, *A&A*, 299, 523
 Frost E. B., Barrett S. B., Struve O., 1926, *ApJ*, 64, 1
 Gagné M., Caillault J.-P., Stauffer J. R., Linsky J. L., 1997, *ApJ*, 478, L87
 Genzel R., Stutzki J., 1989, *ARA&A*, 27, 41
 Harries T. J., 2000, *MNRAS*, 315, 722
 Henrichs H. F. et al., 2002, *A&A*, submitted
 Howarth I. D., Prinja R. K., 1989, *ApJS*, 69, 527
 Howarth I. D., Siebert K. W., Hussain G. A. J., Prinja R. K., 1997, *MNRAS*, 284, 265
 Lucy L. B., White R. L., 1980, *ApJ*, 241, 300
 Mathys G., 1991, *A&AS*, 89, 121

- Mewe R., Kaastra J. S., Liedahl D. A., 1995, *Legacy*, 6, 16
- Morrison R., McCammon D., 1983, *ApJ*, 270, 119
- O'Dell C. R., Yusef-Zadeh F., 2000, *AJ*, 120, 3820
- Owocki S. P., Castor J. I., Rybicki G. B., 1988, *ApJ*, 335, 914
- Pauldrach A., Puls J., Kudritzki R. P., 1986, *A&A*, 164, 86
- Piskunov N. E., 1985, *Pis. AZh*, 11, 44 (*SvA Lett.* 11, 18)
- Plaskett J. S., Pierce J. A., 1924, *Publ. Dom. Ap. Obs.*, 2, 305
- Preston G. W., 1967, *ApJ*, 150, 547
- Reiners A., Stahl O., Wolf B., Kaufer A., Rivinius T., 2000, *A&A*, 363, 585
- Schaller G., Schaerer D., Meynet G., Maeder A., 1992, *A&AS*, 96, 269
- Schulz N. S., Canizares C. R., Huenemoerder D., Lee J. C., 2000, *ApJ*, 545, L135
- Schulz N. S., Canizares C. R., Huenemoerder D., Kastner J. H., Taylor S. C., Bergstrom E. J., 2001, *ApJ*, 549, 441
- Shore S. N., 1999, in Wolf B., Stahl O., Fullerton A. W., eds, *IAU Coll.* 169, *Variable and Non-Spherical Stellar Wind in Luminous Hot Stars*. Springer-Verlag, Berlin, p. 178
- Shore S. N., Brown D. N., 1990, *ApJ*, 365, 665
- Smith M. A., Groote D., 2001, *A&A*, 372, 208
- Stahl O., 1998, in Kaper L., Fullerton A., eds, *Proc. of the ESO Workshop on Cyclical Variability in Stellar Winds*. Springer-Verlag, Berlin, p. 246
- Stahl O., Wolf B., Gang T., Gummertsbach C. A., Kaufer A., Kovacs J., Mandel H., Szeifert T., 1993, *A&A*, 274, L29
- Stahl O. et al., 1996, *A&A*, 312, 539
- Stibbs D. W. N., 1950, *MNRAS*, 110, 395
- Wade G. A., Donati J.-F., Landstreet J. D., Shorlin S. L. S., 2000, *MNRAS*, 313, 851
- Walborn N. R., Nichols J. S., 1994, *ApJ*, 425, L29
- Waldron W. L., Cassinelli J. P., 2001, *ApJ*, 548, L45
- Weigelt G., Balega Y., Preibisch T., Schertl D., Schöller M., Zinnecker H., 1999, *A&A*, 347, L15

This paper has been typeset from a \TeX/L\AA\TeX file prepared by the author.